Paper

Int'l J. of Aeronautical & Space Sci. 17(3), 391–400 (2016)
DOI: http://dx.doi.org/10.5139/IJASS.2016.17.3.391

IJASS
International Journal of Aeronautical and Space Sciences

Performance Enhancement of a Satellite's Onboard Antenna Tracking Profile using the Ground Station Searching Method

Young-Joo Song*

Korea Aerospace Research Institute, Daejeon 34133, Republic of Korea

Jung-Ro Lee**

Korea Advanced Satellite Technology Agency, Daejeon 34133, Republic of Korea

Jihoon Kang*** **, Moon-Jin Jeon****** **and Sang-il Ahn*******

Korea Aerospace Research Institute, Daejeon 34133, Republic of Korea

Abstract

In satellite operations, stable maneuvering of a satellite's onboard antenna to prevent undesirable vibrations to the satellite body is required for high-quality high-resolution images. For this reason, the onboard antenna's angular rate is typically minimized while still satisfying the system requirement that limits the speed of the onboard antenna. In this study, a simple yet effective method, called the ground station searching method, is proposed to reduce the angular rate of a satellite's onboard antenna. The performance of the proposed method is tested using real flight data from the KOMPSAT-3 satellite. Approximately 83% of arbitrarily selected real flight scenarios from 66 test cases show reductions in the onboard antenna's azimuth angular rates. Additionally, reliable solutions were consistently obtained within a reasonably acceptable computation time while generating an onboard antenna tracking profile. The obtained results indicate that the proposed method can be used in real satellite operations and can reduce the operational loads on a ground operator. Although the current work only considers the KOMPSAT-3 satellite as a test case, the proposed method can be easily modified and applied to other satellites that have similar operational characteristics.

Key words: Onboard satellite antenna, Gimbal system, Tracking Profile Generation

1. Introduction

A satellite in low Earth orbit (LEO) is typically equipped with an omnidirectional or directional antenna system to communicate with a ground station (GS). If a satellite is equipped with a directional antenna system, a gimbal system is typically mounted between the body and antenna to maintain focus on a GS. Typically, a set of commands to point the directional antenna system toward the target GS, typically called the tracking profile (TP), is uploaded by ground operators [1, 2]. Similar to other LEO satellites, the KOrea Multi-Purpose SATellite 3 (KOMPSAT-3) also uses the TP to transmit telemetry and image data to Earth. During the process of maneuvering an onboard antenna toward a target GS with a gimbal system, undesirable vibrations can be produced in the satellite body that degrade the quality of high-resolution images by introducing a smearing effect. Although the satellite body itself is designed to reduce these types of vibrations and the onboard antenna's movements are mechanically limited, minimization of these movements is still required even though the systemic requirements to operate a satellite are satisfactorily achieved. As space missions become increasingly complex, movements of onboard antenna must be minimized while still satisfying system requirements;

* Senior Researcher, Corresponding author: dear.yjsong@gmail.com, dearyjs@kari.re.kr
** Research Engineer
*** Senior Researcher
**** Senior Researcher
***** Principal Researcher

Received: March 2, 2015 Revised: March 17, 2016 Accepted: August 1, 2016

http://ijass.org pISSN: 2093-274x eISSN: 2093-2480

furthermore, they must be reliable, sufficiently flexible to adapt to many mission-dependent changes, and cost effective for mission schedulers [3, 4]. In addition, the process of generating commands should effectively reduce the load on ground operators, which is directly related to the automation of highly complex satellite ground systems [5-7], a major interest to associated communities worldwide.

Unlike other studies on mission scheduling problems (e.g., satellite imaging or observation scheduling), the TP for a satellite's onboard antenna has rarely been studied. As described in Refs. [8, 9], a single target GS is used to generate a TP, and the performance enhancement of a TP was continuously investigated to minimize the onboard antenna's speed during pointing GS while satisfying all operational constraints.

To reduce this angular rate, the concept of a virtual GS was proposed [10]. This concept can be applied to real operations by considering the allowable maximum satellite antenna rotation angle that can communicate with the central target GS without signal loss; this angle can then be regarded as the off-pointing margin angle. An extended version of the virtual GS concept is also addressed in [11], in which continuous pointing at moving virtual GSs located on the ground occurs during maneuvering of the onboard antenna. However, performance using this method was only marginally enhanced because maneuvering the onboard antenna to follow pre-defined, half-circle-shaped virtual GSs cannot be widely applied to mission scenarios that have different orbits and attitudes. Various optimization approaches have also been studied, including validation methods to minimize the movement of the onboard antenna [4, 12 – 15]. However, obtaining such an optimum solution with varying parameters in different operational constraints is time consuming and produces high computational loads. One of the important factors that must be considered in TP performance enhancement is that the solution should always be reliably obtained even with different task-dependent constraints. Although various fascinating optimization methods have been proposed and developed, in the real operation of KOMPSAT-3, a TP is generated using the method proposed in Ref. [10], which uses the location of three target GSs to secure the stable operation of the KOMPSAT-3. In Ref. [10], one of the target ground stations is the central KARI Mission Operation Center (KMOC); the other two stations are fixed virtual ground stations located at the east northeast and west southwest sides of the central KMOC; these locations were selected by trial and error during KOMPSAT-3 operation to improve the performance of the satellite's TPs. Although the method described in Ref. [10] reduced the speed of the onboard antenna's movement and addressed all KOMPSAT-3 operational requirements, this method has not been broadly adapted to include various operational tasks because its solutions are limited to target only three GSs.

In this study, a simple yet effective method, called the ground station searching method, is proposed to improve the performance of TP generation. The proposed method aims to minimize the speed of an onboard antenna's movement and to obtain reliable solutions within a reasonable time suitable for actual satellite operations. The performance of the proposed method is tested using real KOMPSAT-3 satellite flight data. Using the proposed method, the currently operational KOMPSAT-3 TP showed performance improvements, and the derived solutions were calculated within an acceptable computation time, which was confirmed by KOMPSAT-3 mission schedulers for numerous test cases. Although the solutions obtained with the proposed method may not be optimal solutions to the problem of interest, they are applicable to wide ranges of real operation scenarios. It is expected that the proposed method can also be applied to TP generation for KARI's next Earth-imaging satellite, KOMPSAT-3A, which is planned to be launched in early 2015. The proposed method can also be easily modified and applied to other LEO satellites that have similar operational restraints. The remainder of this paper is organized as follows. In Section 2, the TP generation process is briefly discussed for the KOMPSAT-3 mission. Detailed algorithms to implement the proposed method are provided in Section 3 with the derivation of antenna gimbal angles and its associated rates, including approaches used to compute virtual GS locations. The virtual GS selection process is also addressed in Section 3. Simulation results are provided with detailed discussions in Section 4, and finally, conclusions are given in Section 5.

2. Brief Review of the Tracking Profile Generation Process

To orient KOMPSAT-3's onboard X-band antenna to GS, a scheduled maneuvering sequence of the X-band antenna is pre-generated and stored in a tracking parameter file (TPF), which is then uploaded to KOMPSAT-3 through the S-band before the task. The TPF is pre-generated by ground operators by running TPF generation software, which is implemented in the image collection planning subsystem (ICPS). During the process of generating a TPF, numerous operational constraints and boundaries on the X-band antenna's gimbal angles and its associated rates, which are limited by the mechanical design of the antenna pointing

mechanism (APM) and the assembled structure attaching it to the satellite body, should be considered. The speed of the onboard antenna's movement should also be minimized throughout the task to prevent undesirable vibrations to the satellite body. These two conditions are required when pre-generating a TPF. It is often difficult to generate a TPF because it must accommodate different satellite orbits, attitudes, positions of the GS, task durations, and numbers and types of sub-tasks (e.g., imaging types, which can be either multi-point or strip; and non-imaging and downlink types, which may be real-time or playback). Thus, the successful generation of a TPF that satisfies all restrictions is necessary to proceed to further mission scheduling. For example, if pre-generation of a TPF is not satisfactorily constructed, ground operators must re-allocate every imaging and downlink schedule using trial and error to meet every user's request regarding their priority after considering long-term schedules; this task is typically time consuming.

Several sequential steps are used to generate an antenna TPF for the KOMPSAT-3 satellite as follows. When the satellite attitude and position with respect to the Earth Centered Earth Fixed (ECEF) frame with numerous mission parameters used to a given formulate mission sequence are available, the preliminary tracking profile can be generated. When computing the preliminary tracking profile, the best target ground station is selected among three different target GSs that minimize the maximum azimuth angular rate throughout the time-varying profiles. Only the azimuth angular rate of the onboard antenna is considered as a major constraint because the elevation angular rate generally does not exhibit dramatic rate changes according to the geometry between the satellite attitude and target station. Based on the preliminary tracking profile, a corrected tracking profile is generated to correct for misalignment errors due to the APM mounting, backlash, RF beam bore-sight, and misalignments with respect to the satellite bus itself. Then, a modified tracking profile is generated by considering the antenna's mechanical and operational limits. During this process, a smoothing algorithm is applied to the specific segment of a sub-task if the associated profile violates mechanical limitations. If smoothing is applied to the derived profile, a loss of communication is again checked using the antenna's effective beam width margin. After the modified tracking profile is successfully generated, coefficients of a 5th-order polynomial are extracted for upload to the satellite [8]. However, before uploading, a TPF is again generated using the extracted coefficients of the 5th-order polynomial, and communication availability is double checked, as shown in Ref. [10]. From these TP generation sequences, the critical phase that directly affects the overall TP performance is shown to be the preliminary tracking profile generation phase. Therefore, the current proposed method is primarily applied and implemented to the stages of generating the preliminary tracking profile. In Fig. 1, the overall flow of the TPF generation process is depicted.

3. Problem Definitions

3.1 Derivation of the antenna gimbal angles and their associated rates

When the satellite position, $\mathbf{r}_{Sat}^{ECEF}$, and GS position, $\mathbf{r}_{GS}^{ECEF}$, in the ECEF frame are given, a normalized position vector from the satellite to the GS expressed in the satellite body frame, $\hat{\mathbf{p}}_{Sat2GS}^{BODY}$, can be obtained as follows [16]:

$$\hat{\mathbf{p}}_{Sat2GS}^{BODY} = \left[\mathbf{Q}_{BODY}^{LVLH}\right]\left[\mathbf{Q}_{LVLH}^{ECI}\right]\left[\mathbf{Q}_{ECI}^{ECEF}\right]\frac{\mathbf{r}_{GS}^{ECEF} - \mathbf{r}_{Sat}^{ECEF}}{\left|\mathbf{r}_{GS}^{ECEF} - \mathbf{r}_{Sat}^{ECEF}\right|} \quad (1)$$

In Eq. (1), the satellite position vector expressed in the ECEF frame, $\mathbf{r}_{Sat}^{ECEF}$, is provided by satellite navigation information. The GS position vector expressed in the ECEF frame, $\mathbf{r}_{GS}^{ECEF}$, can be derived from the longitude, λ_{GS}, geodetic latitude, ϕ_{GS}, and geodetic height, h_{GS}, of the target GS. The direction cosine matrices, $\mathbf{Q}_{ECI}^{ECEF}$ and $\mathbf{Q}_{LVLH}^{ECI}$, are well-known matrices that convert a vector from the ECEF frame to the Earth-Centered-Inertial (ECI) frame and from the ECI frame to the Local Vertical/Local Horizontal (LVLH) frame, respectively. Another transformation matrix, $\mathbf{Q}_{BODY}^{LVLH}$, is the matrix that transforms a vector from the LVLH frame to

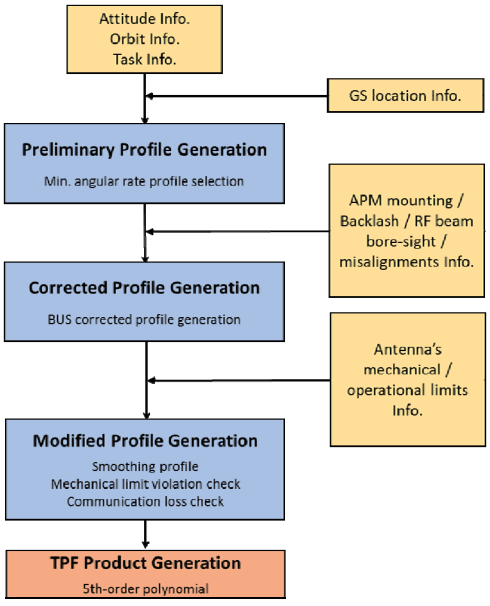

Fig. 1. Overall flow of the TPF generation process.

the satellite body frame, expressed in roll-pitch-yaw Euler angles, which can be obtained from satellite attitude profile.

Using the unit vector $\hat{\mathbf{p}}_{Sat2GS}^{BODY}$, the profile of the antenna gimbal angles, $\alpha(t)$ and $\beta(t)$, which are aimed at the target GS (λ_{GS}, ϕ_{GS}, h_{GS}), can be obtained from Eq. (2). Because the continuously discretized orbit in the ECEF frame and the attitude in the LVLH frame from the satellite navigation information are given, the corresponding profiles of the antenna gimbal angles will also be continuously discretized over time. The geometry of the antenna gimbal angles is shown in Fig. 2.

$$\alpha(t) = \tan^{-1}\left(\frac{\left(\hat{\mathbf{p}}_{Sat2GS}^{BODY}\right)_{j_{Body}}}{\left(\hat{\mathbf{p}}_{Sat2GS}^{BODY}\right)_{i_{Body}}}\right) \tag{2a}$$

$$\beta(t) = \sin^{-1}\left(\left(\hat{\mathbf{p}}_{Sat2GS}^{BODY}\right)_{k_{Body}}\right) \tag{2b}$$

In Eq. (2), $\alpha(t)$ is the azimuth and $\beta(t)$ is the elevation time-varying profile of the onboard X-band antenna. The time derivatives of the azimuth, $\dot{\alpha}(t)$, and elevation, $\dot{\beta}(t)$, of the antenna gimbal angle profile can be derived as follows [15]:

$$\dot{\alpha}(t) = \left[\alpha_1, \alpha_2, ..., \alpha_{n-1}\right] = \left[\frac{\alpha_2 - \alpha_1}{\Delta t}, \frac{\alpha_3 - \alpha_2}{\Delta t}, ..., \frac{\alpha_n - \alpha_{n-1}}{\Delta t}\right] \tag{3a}$$

$$\dot{\beta}(t) = \left[\beta_1, \beta_2, ..., \beta_{n-1}\right] = \left[\frac{\beta_2 - \beta_1}{\Delta t}, \frac{\beta_3 - \beta_2}{\Delta t}, ..., \frac{\beta_n - \beta_{n-1}}{\Delta t}\right] \tag{3b}$$

where n is the total discretized number used to establish a given X-band antenna TP, which may differ for every mission task, and Δt is the sampling interval used to generate a given tracking scenario. A Δt of 1 s is used for all simulations. On-board X-band antenna gimbal angle rates are often mechanically limited and should be operated within their boundaries, as shown in Eq. (4), where the subscripts *min* and *max* indicate pre-defined constraints on the minimum and maximum associated gimbal angle rates, respectively.

$$\dot{\alpha}_{\min} \le \dot{\alpha}(t) \le \dot{\alpha}_{\max} \tag{4a}$$

$$\dot{\beta}_{\min} \le \dot{\beta}(t) \le \dot{\beta}_{\max} \tag{4b}$$

Although these conditions are all satisfied, their variations should still be minimized throughout the tracking operation to prevent undesirable vibrations being transmitted to the satellite body that may degrade the quality of high-resolution images. Only one real target GS will receive a signal from the satellite X-band antenna. However, to reduce gimbal angle rates, the location of an arbitrarily selected virtual GS within the antenna's effective beam width margin could be used to minimize the undesirable vibrations of the satellite body, as shown in Ref. [10].

3.2 Derivation of the virtual ground station distributions

If the longitude, latitude and height of the center point, which is the real GS (λ_0, ϕ_0, h_0), are given, then a square-shaped distribution of the virtual GS location (λ_i, ϕ_j, h_v) with respect to (λ_0, ϕ_0, h_0) can be obtained, where i=1, 2, ..., m, j=1, 2, ..., m and m is a user-defined division number to create equally spaced grids on both longitude and latitude for the virtual GSs. h_v is the height of the virtual GS, which is assumed to always be zero in this study. In real situations, the height of the GS is not always zero; however, unlike the actual GS height, h_0, this assumption is valid for the current study as it focuses on the generation of virtual GS distributions in which transmitted signals from the satellite are received depending on the antenna's effective beam width margin.

The location of the given four edges of square (λ_k, ϕ_l, h_v), where k=1, m. l=1. m and h_v=0, can be approximated by Eq. (5):

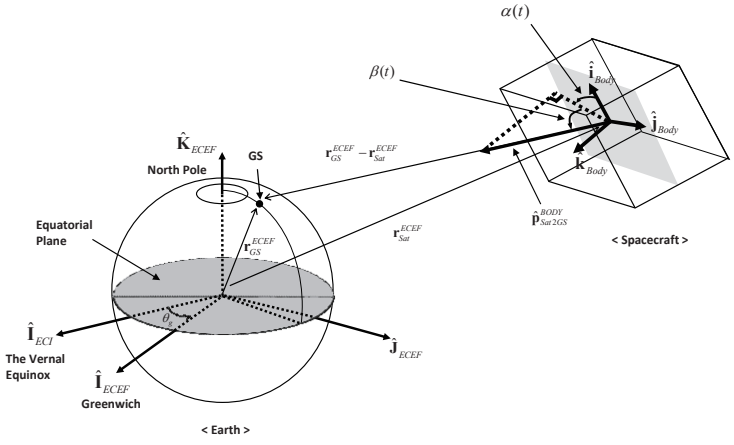

Fig. 2. Geometry of an antenna gimbal angle with respect to the satellite body and ECI frame (not to scale).

$$\lambda_k = \lambda_0 + d_{ang}\sin(\theta) \tag{5a}$$

$$\phi_\ell = \phi_0 + d_{ang}\cos(\theta) \tag{5b}$$

where θ is the defined phase angle to locate the four edges. If k=1 and l=1, then θ=315°; if both k and l are equal to m, then θ=135° is used. Additionally, d_{ang} is the angular distance between (λ_0, ϕ_0, h_0) and each edge's location (λ_k, ϕ_l, h_v), which can be approximated by

$$d_{ang} = \frac{d_{hyp}}{r_\oplus} \tag{6}$$

where d_{hyp} is the hypotenuse distance defined as $d_{hyp} = \sqrt{d_{\max}^2 + d_{\max}^2}$. d_{max} is a user-defined distance, where d_{max}=h_{sat} tan(ψ), which is considered to be the maximum allowable distance to off-point the onboard antenna.h_{sat} is the altitude of the satellite, and ψ is the maximum allowable off-point angle of the onboard antenna. Additionally, $r_\oplus$ is Earth's mean radius, which is 6,378.137 km. d_{max} may have slightly different values depending on the satellite's attitude, the ground projected beam pattern of the onboard antenna, and the shape of the ground antenna's beam. However, this study assumed a simplified model, as was implemented in the KOMPSAT-3 TPF to focus on the performance enhancement introduced by the proposed method. With a given m, the change in longitude and latitude for each grid point can be derived as

$$\Delta\lambda = \frac{\lambda_m - \lambda_1}{m-1} \tag{7a}$$

$$\Delta\phi = \frac{\phi_1 - \phi_m}{m-1} \tag{7b}$$

Then, the matrix that contains the equally distributed virtual GS locations, $M_{ij}(\lambda_i, \phi_j, h_v)$, can be computed as follows:

$$\boldsymbol{M}_{ij}(\lambda_i,\phi_j,h_v) = \begin{bmatrix} (\lambda_1,\phi_1,h_v) & (\lambda_1,\phi_2,h_v) & \cdots & (\lambda_1,\phi_m,h_v) \\ (\lambda_2,\phi_1,h_v) & & & \vdots \\ \vdots & & & \vdots \\ (\lambda_m,\phi_1,h_v) & (\lambda_m,\phi_2,h_v) & \cdots & (\lambda_m,\phi_m,h_v) \end{bmatrix} \tag{8a}$$

$$\lambda_i = \lambda_1 + i\Delta\lambda \quad \text{for} \quad i = 1,\ldots,m \tag{8b}$$

$$\phi_j = \phi_1 + j\Delta\phi \quad \text{for} \quad j = 1,\ldots,m \tag{8c}$$

Then, a single row matrix that contains the coordinates of candidate GS locations, $M_c(\lambda_c, \phi_c, h_v)$, can be extracted from $M_{ij}(\lambda_i, \phi_j, h_v)$ if the conditions shown in Eq. (9) are satisfied. Conditions in Eq. (9) indicate that the candidate GS locations should always be located within the allowable off-point distance of the onboard antenna.

$$d_{ij} \le d_{\max} - d_{mar} \tag{9}$$

where d_{ij} is the distance between (λ_0, ϕ_0, h_0) and the ij^{th} virtual station location in $M_{ij}(\lambda_i, \phi_j, h_v)$, and d_{mar} is the user-provided marginal distance associated with $d_{\max}$ for operational safety. As the number of candidate GSs, c, is increased in each step when Eq. (9) is satisfied, a total of mc candidate GSs will be selected and augmented in $M_c(\lambda_c, \phi_c, h_v)$ out of the m×m distributed virtual GS locations, $M_{ij}(\lambda_i, \phi_j, h_v)$. To compute d_{ij} in Eq. (9), the well-known method described in Ref. [17] is directly adapted.

3.3 Final target ground station selection

Among the total of mc candidate GSs, $M_c(\lambda_c, \phi_c, h_v)$, the coordinates of the final virtual target GS, (λ_{tar}, ϕ_{tar}, h_v), should be selected so that the maximum magnitude of the azimuth angular rate obtained with the c^{th} candidate GS, $\dot{\alpha}_c(t)$, is minimized during the given pointing task, which is described by the following condition:

$$(\lambda_{tar},\phi_{tar},h_v) = \boldsymbol{M}_c(\lambda_c,\phi_c,h_v) \quad \text{if} \quad \min\left[\max\left[\left|\dot{\alpha}_c(t)\right|\right]\right] \quad \text{for} \quad c = 1,\ldots,mc \tag{10}$$

Then, the selected virtual target GS will be the final GS, (λ_{GS}, ϕ_{GS}, h_{GS})=(λ_{tar}, ϕ_{tar}, h_v), at which the satellite onboard antenna should point. With this selected final target GS, the highest-performing TP for the given task will be shown. In Eq. (10), only the magnitude of the azimuth angular rate of the onboard antenna is minimized during the final target ground station selection process because the elevation angular rate variation typically does not undergo rapid changes, as opposed to the azimuth angular rate, due to the geometries between the satellite's orbit, attitude and the locations of the GS during LEO flight operations. The geometrical concept of the proposed virtual GS location derivation is shown in Fig. 3.

4. Results with Real Flight Data

4.1 Simulation Setups

To analyze the results of this study, the proposed method is directly implemented in the real operational TP generation software of the KOMPSAT-3 satellite. A total of 66 real operational scenarios currently used in the KOMPSAT-3 mission are randomly chosen by mission schedulers to determine how this newly implemented method enhances TP performance. Every selected test scenario uses different satellite attitude and orbital information, overall task durations, imaging and downlink types with different

durations. In these simulations, the Daejeon site is considered as the target station; however, the proposed method can be modified and applied to any GS's location to derive a TP. The location of the center GS is given to be approximately 127.35 deg E, 36.38 deg N at a height of 110 m. To create equally spaced grids in both longitude and latitude for the virtual GSs, m is set to be 20 by trial and error while considering computational time and TP performance enhancements. Additionally, candidate GS locations are selected with the conditions of d_{max}-d_{mar}=250 km, as shown in Eq. (9). This value is selected as the current two virtual ground stations, as implemented in the ICPS for the KOMPSAT-3 satellite, and are located approximately 250 km apart from the central KMOC, which is located in Daejeon City. Before discussing the primary analysis results, the maximum azimuth angular rate of the onboard antenna is derived using both the current method (i.e., method A) and the method presented in Ref. [10] (i.e., method B). For method B, two virtual GSs locations are given; the ENE virtual GS is located at approximately 129.80 deg E, 36.78 deg N, and the WSW virtual GS is located at approximately 125.08 deg E, 35.78 deg N (ENE and WSW indicate the compass directions East-North-East and West-South-West, respectively).

4.2 Analysis of the Results

Before deriving a TP for each mission scenario given, the first step is to find the candidate virtual GSs among the distributed virtual GSs. Among the 400 distributed virtual GSs, a total of 328 candidate virtual GSs satisfy the conditions shown in Eq. (9) and are thus selected for further consideration. As expected, the candidate virtual GSs are equally distributed with respect to the central real GS, as shown in Fig. 4. However, some selected target virtual GSs are located in the territory of North Korea. Though the downlink signal is encoded, these problems can easily be solved by additionally constraining the latitude conditions during the process of selecting candidate virtual GSs with the conditions shown in Eq. (9). However, because the proposed method has not been verified for actual flight operation, constraints on the latitude conditions are not considered in the following analysis.

After selecting candidate virtual GSs, a near-optimum target GS is selected from the 328 candidate virtual GSs for each of the 66 test scenarios; these target GSs minimize the magnitude of the maximum azimuth angular rate of the onboard antenna. When compared to the solutions derived with method B, a total of 55 scenarios (approximately 83%) show improvement in their tracking profile's performance by adapting method A. For the remaining scenarios, the generated tracking profile with method B showed a lower maximum azimuth angular rate than the minimized values produced by method A. This indicates that targeting the ENE

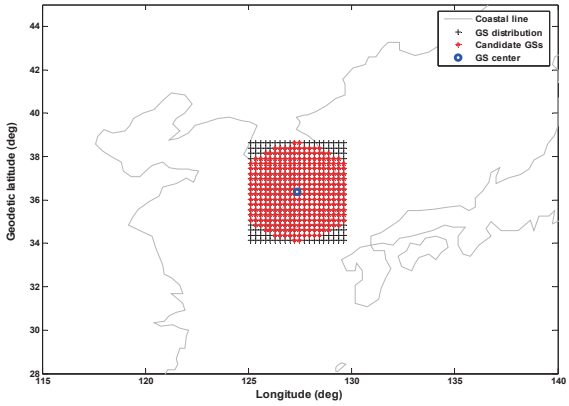

Fig. 4. Candidate GSs' distribution with respect to the GS center.

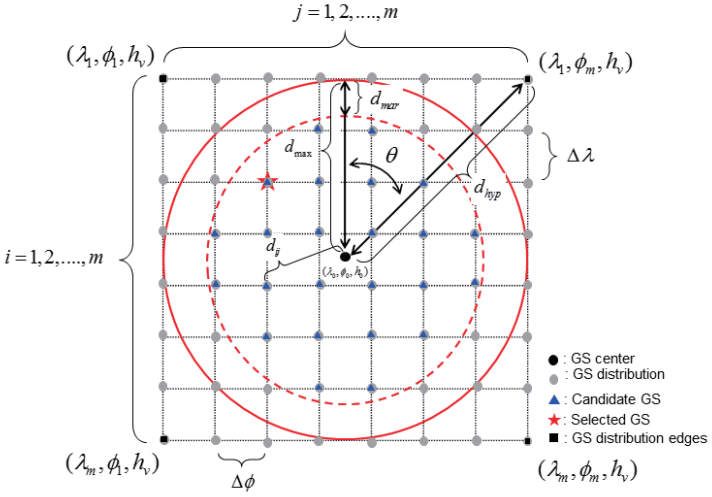

Fig. 3. Geometrical concept of the proposed virtual GS location derivation (not to scale).

or WSW virtual GS or the central GS is better than targeting the virtual GSs (328 candidate virtual GSs) generated with method A. Table 1 lists the top 10 test cases out of the 55 scenarios that showed performance improvements. In Table 1, enhanced performance is directly compared as percentage rates using the maximum azimuth angular rates of the onboard antenna derived from methods A and B. In the top 10 cases shown in Table 1, more than approximately 12% of the maximum azimuth angular rates are reduced in magnitude by using the current method; a maximum reduction of approximately 25% is also achieved. Additionally, the mean of the rate reductions for the 55 scenarios is approximately 11.46%. These improvements are noticeable reductions, especially considering that the proposed method is sufficiently simple, reliable and fast to be used in real operations. As shown in Table 1, the computational time of method A is approximately 0.4-2.4 min (0.1-2.6 min for all 66 test scenarios); this is several minutes slower than the computation time required with method B, which all remained less than 1 min. Although slower than method B, we have confirmed from the operator of the KOMPSAT-3 satellite that the observed computation times are tolerable when scheduling tasks; therefore, they do not significantly hinder overall mission operation. In addition, within the ranges of computation times in method A, operators have confirmed that obtaining stable and reliable solutions with given scheduled tasks is the most important factor in this process due to significant changes in initial orbit conditions, attitudes, overall task duration and the durations of each sub-task; stable and reliable solutions were rare with the previous method that utilized optimization algorithms.

In Fig. 5, the locations of the selected virtual GSs produced by method A are depicted for the top 10 performing scenarios; two of the virtual GSs used to derive the TP produced by method B are also marked for comparison. As an example, cases 1 and 2 identified the ENE virtual GS (125.08 deg E, 35.78 deg N) to minimize the azimuth angular rate of the onboard antenna using method B; however, after applying method A, the targeting locations for the onboard antenna were moved slightly to the northwest with respect to the central GS for case 1 and moved to the south for case 2. The corresponding coordinates for the selected virtual GSs using the current method are 125.11 deg E, 36.97 deg N for case 1, and 127.24 deg E, 34.13 deg N for case 2. These slight changes in the target virtual GSs' locations reduced the azimuth angular rate of the onboard antenna by approximately 25% for case 1 and approximately 18% for case 2, which could

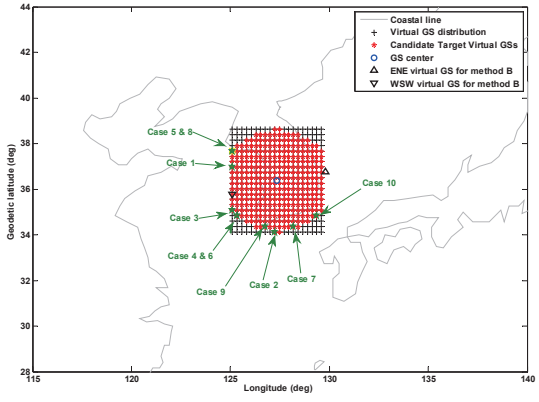

Fig. 5. Location of the selected virtual GSs for the top 10 performing cases that minimize the maximum azimuth angular rate of the onboard antenna's movement using method A.

Table 1. Derived maximum azimuth angular rates of methods A and B. Top 10 performing cases from the 55 scenarios that showed enhanced performance.

Test cases	Max. azimuth angular rate magnitude (deg/s)				Computing time (min)	
	With method A ①	With method B ②	Reduced max. azimuth angular rate (deg/s) ②-①	Performance Improvement (%) ((②-①)/②) x 100	With method A	With method B
1	1.77	2.37	0.60	25.19	2.37	0.16
2	0.59	0.72	0.13	17.69	1.31	0.09
3	0.04	0.05	0.01	17.37	0.29	0.04
4	0.10	0.12	0.02	17.17	0.40	0.06
5	0.51	0.59	0.08	12.63	2.07	0.13
6	0.07	0.08	0.01	12.62	1.21	0.11
7	0.02	0.03	0.01	12.35	0.49	0.06
8	1.23	1.40	0.17	11.99	1.43	0.13
9	0.27	0.31	0.04	11.81	0.54	0.06
10	0.10	0.12	0.02	11.69	0.35	0.04

seriously affect the quality of a high-resolution image. In Table 2, the locations of the selected target virtual GSs with method A are listed for the top 10 performing cases and compared to the solutions produced by method B. The characters in Table 2 are defined as follows: N for north, S for south, E for east, W for west and C for central. By applying method A, the locations of the target virtual GSs are changed to the locations where they can minimize the maximum angular rate of the onboard antenna under given mission tasks.

In Figures 6 and 7, the variation profiles of the onboard antenna's azimuth angular rate for methods A and B are compared for case 1 (Fig. 6) and case 2 (Fig. 7). Case 1 has a task duration of 625 s and is composed of 13 different sub-tasks: the imaging of a target area with a real-time data downlink and playback data downlink. For case 2, 7 different sub-tasks are implemented over a task duration of 357 s. In addition, near the peaks in both figures, rapid satellite attitude reorientations are shown to perform the given sub-mission tasks. As shown in Fig. 6, the magnitude of the minimized maximum value for the azimuth angular rate was found to be approximately 2.37 deg/s approximately 345 s after the beginning of the task with method B and approximately 1.77 deg/s approximately 374 s after the task began with method A. For case 2, shown in Fig. 7., the minimized maximum azimuth angular rate magnitude with method A was approximately 0.59 deg/s approximately 57 s after the task began and approximately 0.72 deg/s approximately 57 s after the task began with method B during the task. Although variation in the elevation angular rate is not of

Table 2. Location comparisons of the selected target virtual GSs between methods A and B.

Test cases	With method A			With method B		
	Latitude (deg)	Longitude (deg)	Virtual GS direction w.r.t. central GS	Latitude (deg)	Longitude (deg)	Virtual GS direction w.r.t. central GS
1	36.97 N	125.11 E	NW	36.78 N	129.80 E	ENE
2	34.13 N	127.24 E	S	36.78 N	129.80 E	ENE
3	35.08 N	125.11 E	SW	36.78 N	129.80 E	ENE
4	34.84 N	125.35 E	SW	36.78 N	129.80 E	ENE
5	37.68 N	125.11 E	NW	36.78 N	129.80 E	ENE
6	34.84 N	125.35 E	SW	36.78 N	129.80 E	ENE
7	34.37 N	128.18 E	SSE	36.38 N	127.35 E	C
8	37.68 N	125.11 E	NW	36.78 N	129.80 E	ENE
9	34.37 N	126.76 E	SSW	36.78 N	129.80 E	ENE
10	34.84 N	129.36 E	SE	35.78 N	125.08 E	WSW

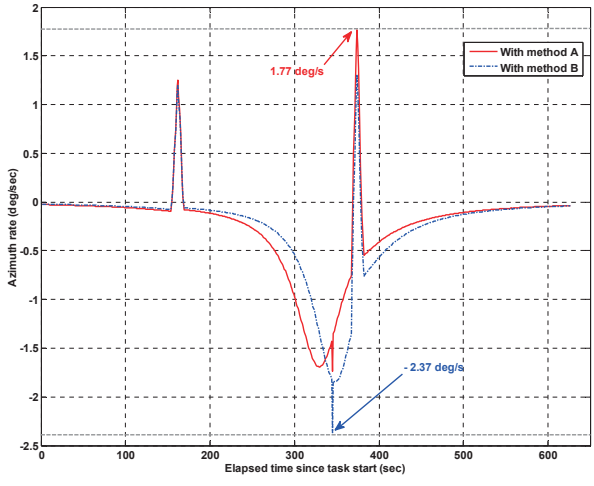

Fig. 6. Azimuth angular rate variation profile comparison for case 1 between methods A and B.

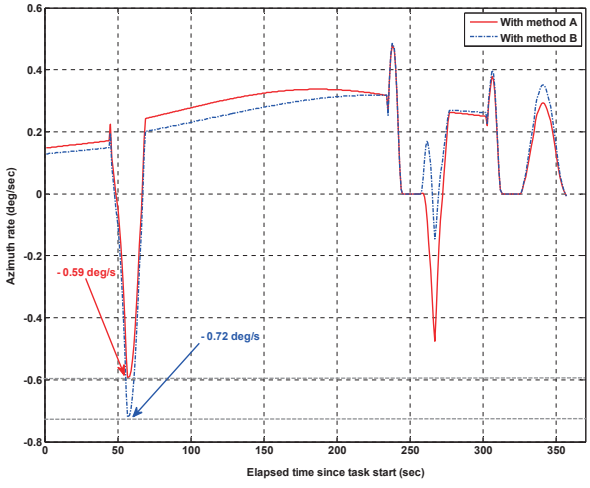

Fig. 7. Azimuth angular rate variation profile comparison for case 2 between methods A and B.

DOI: http://dx.doi.org/10.5139/IJASS.2016.17.3.391

primary interest in this study and is therefore not shown, the magnitude of the maximum elevation angular rate throughout the task was also reduced by applying method A to case 1. For case 2, no significant differences in the variation histories of the elevation angular rate were observed between methods A and B. The magnitudes of both the maximum azimuth and elevation angular rates with methods A and B were significantly lower than the mechanical limitations (Eq. (4)) imposed on the KOMPSAT-3 satellite; thus, these rates satisfied the systemic design requirements. However, the reduced gimbal angle rates produced by method A will remove undesirable vibrations in the satellite body during the performance of mission tasks.

5. Conclusions

In this paper, a ground station searching method is proposed to reduce the angular rates of a satellite's onboard antenna during tracking profile generation. A tracking profile should be stably generated rapidly, and the associated speed of the onboard antenna's movement to point at a given target ground station should be minimized to reduce undesirable vibrations to the satellite body, avoiding degradation of the quality of high-resolution imaging. Therefore, the proposed method is founded upon the motivations of minimizing the speed of the onboard antenna's movement while obtaining reliable solutions within a reasonable time that is suitable for real satellite operation. To validate the performance of the proposed method, 66 real mission scenarios of the KOMPSAT-3 satellite are arbitrarily selected and analyzed. Approximately 83% of these flight scenarios show reductions in their onboard antenna's azimuth angular rates. Additionally, reliable solutions were always obtained within a reasonable computation time of less than several minutes when generating the tracking profile. Although proposed method of generating the tracking profile is slightly slower than the method currently adapted for real operation of KOMPSAT-3, the operator has confirmed that such a delay in computation time does not affect the overall mission operation. By adapting the proposed method, a maximum of approximately 25% of the maximum azimuth angular rates are reduced in magnitude when compared to the solutions obtained from the method currently used during the operation of the KOMPSAT-3 satellite. These improvements are significant reductions, particularly when considering the simplicity, reliability and sufficiently fast computing time, which can be used in real satellite operations. In future work, the effects on the quality of high-resolution imaging produced by the reductions in speed achieved with the proposed method should be analyzed in more detail. The authors believe that the proposed method could also be applied to tracking profile generation for KARI's next Earth imaging satellite, the KOMPSAT-3A, which is planned to be launched in early 2015. Moreover, the proposed method could be easily modified and applied to other LEO satellites with similar operational concepts.

Acknowledgments

This work was performed by the Korea Aerospace Research Institute (KARI) under a contract with the Ministry of Science, ICT and Future Planning (MSIP) through the "Development of Pathfinder Lunar Orbiter and Key Technologies for the Second stage Lunar Exploration" project (No. SR16023).

References

[1] Bagchi, T. P., "Near Optimal Ground Support in Multi-spacecraft Missions: a GA Model and its Results", *IEEE Transactions on Aerospace Electronic Systems*, Vol. 45, No. 3, 2009, pp. 950–964.

[2] Noll, J. and Steel, R., "EKLOPS: an Adaptive Approach to a Mission Planning System", *Proceedings of the IEEE Aerospace Conference*, Big Sky, Montana, 2005.

[3] Chouinard, C., Knight, R., Jones, G. and Tran, D., "Orbital Express Mission Operations Planning and Resource Management Using ASPEN", *Proceedings of the SPIE6958, Sensors and Systems for Space Applications II*, Orlando, Florida, 2008.

[4] Lee, J. G., Ahn, H. S., Ko, K. H., Wang, S., Jung, O. C., Choi, S. J. and Chung, D., "Generation of Satellite Tracking Profile: Problems and Validation Algorithms", *Advances in Space Research*, Vol. 54, No. 6, 2014, pp. 1092-1107.

[5] Wang, P. and Chen, J., "Research and Implementation of Ground Station Software System with Highly Automation", *Proceedings of the SPIE5985, International Conference on Space Information Technology*, Wuhan, China, 2005.

[6] Maurer, E., Mrowka, F., Braun, A., Geyer, M. P., Lenzen, C., Wasser, Y. and Wickler, M., "TerraSAR-X Mission Planning System: Automated Command Generation for Spacecraft Operations", *IEEE Transactions on Geoscience and Remote Sensing*, Vol. 48, No. 2, 2010, pp. 642–648.

[7] Firestone, D., Atkin, R., Hooks, C., Englert, C. R., Siskind, D. E, Bernhardt, P. A., Siefring, C. L. and Klein, P. A., "Low-cost, Automated Ground Station for LEO Mission Support", *IEEE Aerospace and Electronic Systems Magazine*,

Vol. 26, No. 3, 2011, pp. 12–18.

[8] Choi, S. J., Jung, O. C., Kang, C. H., Kim Y. O. and Chung, D. W., "An Algorithm to Eliminate TPF Discontinuity for LEO Satellite", *Proceedings of Annual Conference of the Korean Society for Aeronautical and Space Science*, Pyungchang, Republic of Korea, 2009.

[9] Jung, O. C., Kim, H. D., Ahn S. I. and Kim E. K., "An Analysis of the Onboard Antenna Tracking Considering Orbital Motion", *Proceedings of Annual Conference of the Korean Society for Aeronautical and Space Science*, Pusan, Republic of Korea, 2006.

[10] Choi, S. J., Ahn, H. S., Kang, C. H. and Jung, O. C., "Design of Off-pointing Tracking Profile and its Validation Algorithm for Directional Antenna", *Proceedings of Asia-pacific International Symposium on Aerospace Technology*, Jeju, Republic of Korea, 2010.

[11] Jeon, M. J., Choi, S. J., Kim, H. S. and Choi, H. J., "Modified TPF Generation Algorithm Using Ground Contour Tracking Method", *Proceedings of International Symposium on Remote Sensing*, Incheon, Republic of Korea, 2012.

[12] Ahn, H. S., Chung, D., Ko, K. H., Wang, S. Jung, O. C. and Choi, S., "Satellite Antenna Control: Design and Performance Validation Under Given TPF", *Proceedings of International Conference on Control, Automation and systems*, KINTEX, Republic of Korea, 2010.

[13] Ahn, H. S., Jung, O. C., Choi, S. J., Son, J. H., Chung, D. and Kim, G., "An Optimal Satellite Antenna Profile Using Reinforcement Learning", *IEEE Transactions on systems, Man, and Cybernetics, Part C: Application and Reviews*, Vol. 41, No. 3, 2011, pp. 393-406.

[14] Lee, D., Lee, K. M., Rashed, M. I. and Bang, H., "An Antenna Tracking Profile Design for Communication with a Ground Station", *International Journal of Aeronautical and Space Science*, Vol. 14, No. 3, 2013, pp. 282-295.

[15] Lee, J. G., Ahn, H. S., Ko, K. H., Wang S., Kim, D. W., Choi, S. J., Jung, O. C. and Chung, D. W., "Profile Optimization of Satellite Antenna for Angular Jerk Minimization", *Proceedings of 12th International Conference on Space Operations*, Stockholm, Sweden, 2012.

[16] Vallado, D. A., *Fundamentals of Astrodynamics and Applications 4th ed.*, Microcosm Press, Hawthorne, 2013.

[17] Sodano, E. M., "General Non-iterative Solution of the Inverse and Direct Geodetic Problems", Bulletion Geodesique, Vol. 75, No. 1, 1965, pp. 69-89.